

Quantum Selection of Order in an XXZ Antiferromagnet on a Kagomé Lattice

A. L. Chernyshev¹ and M. E. Zhitomirsky²

¹*Department of Physics and Astronomy, University of California, Irvine, California 92697, USA*

²*Service de Physique Statistique, Magnétisme et Supraconductivité,
UMR-E9001 CEA-INAC/UJF, 17 rue des Martyrs, 38054 Grenoble Cedex 9, France*

(Dated: August 5, 2022)

Selection of the ground state of the kagomé-lattice XXZ antiferromagnet by quantum fluctuations is investigated by combining non-linear spin-wave and real-space perturbation theories. The two methods unanimously favor $\mathbf{q}=0$ over $\sqrt{3}\times\sqrt{3}$ magnetic order in a wide range of the anisotropy parameter $0 \leq \Delta \lesssim 0.72$. Both approaches are also in an accord on the magnitude of the quantum order-by-disorder effect generated by topologically non-trivial, loop-like spin-flip processes. A tentative S - Δ phase diagram of the model is proposed.

PACS numbers: 75.10.Jm, 75.30.Ds, 75.50.Ee, 75.45.+j

Kagomé-lattice antiferromagnets (KGAFMs) are central to theoretical and experimental studies in frustrated magnets. They host long-sought magnetically disordered spin-liquids and intriguing valence-bond solids, exhibit order-by-disorder phenomena, and are dominated by unconventional excitations [1–26]. Many of these remarkable properties take their root in a massive degeneracy of the ground state of the classical kagomé nearest-neighbor Heisenberg model. The degeneracy can be lifted by thermal or quantum fluctuations, or by secondary interactions. Because of experimental realizations, order selection by the symmetry-breaking Dzyaloshinskii-Moriya (DM) terms has been intensely studied [27–35] and so has been the effect of further-neighbor couplings [2], which lift the degeneracy within the manifold of classical 120° states. Two of such states, the $\sqrt{3}\times\sqrt{3}$ and the $\mathbf{q}=0$ spin patterns, are the main contenders for the ground state from the quasiclassical perspective, see Figs. 1(a,b).

On the other hand, studies of quantum effects have been concentrated on the Heisenberg case where most methods offer only limited insight into *how* the ground state is selected. In this work, we address the problem of order-by-disorder (ObD) by quantum fluctuations in KGAFMs using the XXZ version of the nearest-neighbor, spin- S model

$$\hat{\mathcal{H}} = J \sum_{\langle ij \rangle} \left(S_i^x S_j^x + S_i^y S_j^y + \Delta S_i^z S_j^z \right), \quad (1)$$

where anisotropy is of the easy-plane type, $0 < \Delta < 1$. It is important to note that the degeneracy among the 120° coplanar states of the classical XXZ KGAFM remains *the same* as in the Heisenberg limit, $\Delta=1$. Therefore, by extending the parameter space without explicitly lifting degeneracy of the classical ground-state manifold we are able to provide deeper insight into the quantum ObD effect. More specifically, we shed light on the mechanism by which the choice is made between $\mathbf{q}=0$ and $\sqrt{3}\times\sqrt{3}$ ordered patterns in KGAFMs and present a rare example of the situation when quantum ObD defies the general trend and yields the ground state that is different from

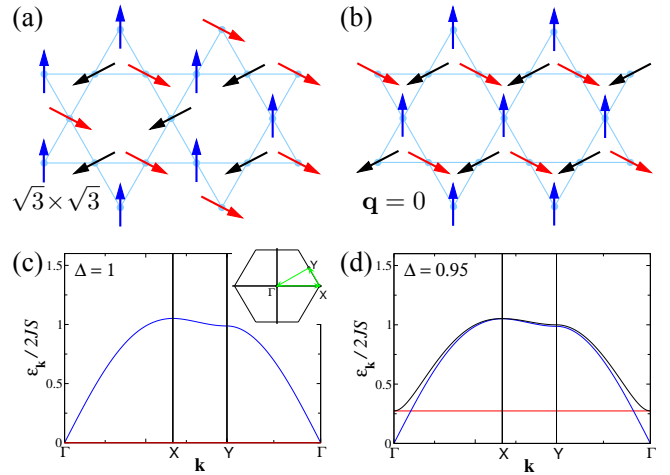


FIG. 1: (Color online) (a) $\sqrt{3}\times\sqrt{3}$ and (b) $\mathbf{q}=0$ spin configurations. Dispersions of spin excitations within the harmonic approximation for (c) $\Delta=1$, and (d) $\Delta=0.95$.

the one favored by thermal fluctuations.

On the technical side, we take advantage of the fact that the so-called “flat mode,” the branch of localized linear spin-wave excitations which has zero energy in the Heisenberg limit, see Fig. 1(c), becomes gaped for $\Delta < 1$ with $\varepsilon_{\mathbf{k}} \propto \sqrt{1-\Delta}$, see Fig. 1(d). Because of that, a controlled $1/S$ expansion becomes possible in the XXZ KGAFM, allowing for a detailed investigation of the quantum selection of the ordered state [36].

Another method that allows for an effective treatment of the highly-degenerate frustrated spin systems is the real-space perturbation theory (RSPT). Applied to the KGAFMs, it operates directly within the manifold of classical 120° states and, by analyzing terms of various order of the perturbation, creates an intuitively transparent real-space hierarchy of effective couplings that are responsible for the ground-state selection. As we show below, it is the convolution of the two methods, $1/S$ expansion and RSPT, which is especially insightful.

Non-linear spin-wave theory (SWT).—For any ordered state from the coplanar 120° manifold one can rewrite (1)

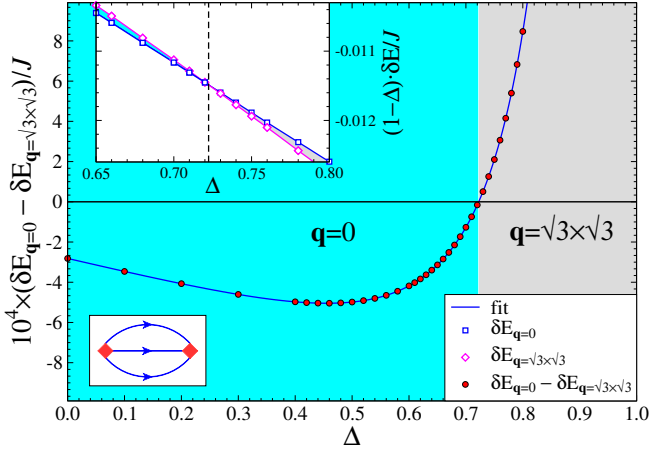


FIG. 2: (Color online) Difference of the ground-state energies (3) of the $\mathbf{q}=0$ and $\sqrt{3} \times \sqrt{3}$ states, per spin. Upper inset: energy correction $\delta E^{(3)}$ for the $\mathbf{q}=0$ (squares) and $\sqrt{3} \times \sqrt{3}$ (diamonds) states. Dashed line marks the transition. Lower inset: diagram for $\delta E^{(3)}$ term in the energy expansion.

in a rotating local basis as

$$\hat{\mathcal{H}} = J \sum_{\langle ij \rangle} \left(\Delta S_i^y S_j^y + \cos \theta_{ij} (S_i^x S_j^x + S_i^z S_j^z) + \sin \theta_{ij} (S_i^z S_j^x - S_i^x S_j^z) \right), \quad (2)$$

where $\theta_{ij} = \theta_i - \theta_j$. Clearly, it is only the last term in (2) which is able to distinguish between different 120° spin configurations by virtue of containing $\sin \theta_{ij} = \pm \sqrt{3}/2$ for the clockwise or counterclockwise spin rotation. This term corresponds to the non-linear, cubic coupling of spin-waves and does not contribute to the linear SWT. Consider the $1/S$ expansion of the ground-state energy

$$E = E_{\text{cl}} + \langle \mathcal{H}_2 \rangle + \langle \mathcal{H}_4 \rangle + \delta E^{(3)} + \dots, \quad (3)$$

where the first term is the classical energy $\mathcal{O}(S^2)$, the second is the linear SWT correction $\mathcal{O}(S)$, and the last two are the contribution of the quartic and cubic terms, both $\mathcal{O}(1)$. It is easy to see from (2) that quartic terms are also unable to differentiate between 120° structures, leaving the cubic term as a sole source of the quantum ObD effect to this $1/S$ order. The energy correction from the cubic terms is represented by the diagram in the lower inset of Fig. 2 and is given by

$$\delta E^{(3)} = -\frac{1}{6N} \sum_{\nu\mu\eta} \sum_{\mathbf{q},\mathbf{k}} \frac{|V_{\mathbf{q},\mathbf{k},-\mathbf{k}-\mathbf{q}}^{\nu\mu\eta}|^2}{\varepsilon_{\mathbf{q}}^\nu + \varepsilon_{\mathbf{k}}^\mu + \varepsilon_{-\mathbf{k}-\mathbf{q}}^\eta}, \quad (4)$$

where ν, μ, η numerate spin-wave branches with harmonic energies $\varepsilon_{\mathbf{k}}^\alpha$ and the cubic vertex comes from the anharmonic part of the spin-wave Hamiltonian

$$\hat{\mathcal{H}}_3 = \frac{1}{3!} \sum_{\nu\mu\eta} \sum_{\mathbf{q},\mathbf{k}} V_{\mathbf{q},\mathbf{k},-\mathbf{k}-\mathbf{q}}^{\nu\mu\eta} b_{\nu,\mathbf{q}}^\dagger b_{\mu,\mathbf{k}}^\dagger b_{\eta,-\mathbf{k}-\mathbf{q}}^\dagger + \text{H.c.} \quad (5)$$

As is clear from previous discussion, this vertex has *different* form for different ordered structures and should be obtained from the spin-wave expansion for each specific 120° spin pattern.

For the linear SWT of the XXZ model (2), we generalize the approach of [2], which has suggested a two-step diagonalization procedure consisting of the unitary transformation of the unit-cell bosons followed by the Bogolyubov transformation for each mode. With that we are able to obtain cubic vertices (5) for the $\mathbf{q}=0$ and $\sqrt{3} \times \sqrt{3}$ states in a fully analytic and elegant form [37], which permit high-accuracy numerical integration in (4) and allow to study quantum ObD effect. The results of such calculations are presented in Fig. 2.

Our main result is the quantum selection of the $\mathbf{q}=0$ state over the $\sqrt{3} \times \sqrt{3}$ counterpart for anisotropy values extending from the XY limit, $\Delta = 0$, to the transition point $\Delta_c \approx 0.72235$. This is contrary to the common belief that quantum fluctuations follow the same selection trend as thermal ones. Indeed, the asymptotic selection of the $\sqrt{3} \times \sqrt{3}$ magnetic structure by thermal fluctuations for the classical KGAFM in both the Heisenberg [38, 39] and the XY limits [40–42] shows no change in the ordering pattern as a function of Δ in contrast to the behavior of the quantum model in Fig. 2. Although the $1/S$ energy correction diverges as $(1 - \Delta)^{-1}$, signifying a failure of the expansion for $\Delta \rightarrow 1$, our results leave little doubt that the $\sqrt{3} \times \sqrt{3}$ state should remain the ground state in the entire range $\Delta_c < \Delta \leq 1$. Previously, a self-consistent spin-wave treatment of the Heisenberg limit [4] has provided an indirect evidence in favor of the $\sqrt{3} \times \sqrt{3}$ ground state for $S \gg 1$. Here this result is strongly implied by a direct calculation of the ground-state energy. Lastly, we observe that the energy gain from the quantum ObD effect is only a fraction of $10^{-3}J$ per spin.

Real-space perturbation theory.—What is the mechanism of quantum selection of the ground state? We address this question using the RSPT [43–46]. This approach divides the Hamiltonian (2) into an unperturbed part $\hat{\mathcal{H}}_0 = h \sum_i (S - S_i^z)$, describing spin fluctuations in the local field $h = 2JS$, and perturbation \hat{V} , which couples fluctuations on adjacent sites. Then, the standard perturbation theory is used to calculate quantum corrections to the classical ground-state energy. The coupling between spin fluctuations contains four terms $\hat{V} = \sum_{i,j} (\hat{V}_1^{ij} + \hat{V}_2^{ij} + \hat{V}_3^{ij} + \hat{V}_4^{ij})$

$$\begin{aligned} \hat{V}_1^{ij} &= -A_+ (S_i^+ S_j^+ + \text{H.c.}), & \hat{V}_2^{ij} &= 2A_- S_i^+ S_j^-, & (6) \\ \hat{V}_3^{ij} &= -B_{ij} \delta S_i^z (S_j^+ + S_j^-), & \hat{V}_4^{ij} &= -C \delta S_i^z \delta S_j^z, \end{aligned}$$

where we introduce $\delta S_i^z = S - S_i^z$, $A_\pm = J(\Delta \pm 1/2)/8$, $B_{ij} = J \sin \theta_{ij}/2$, $C = J/4$, and keep $\sin \theta_{ij} = \pm \sqrt{3}/2$ in \hat{V}_3 explicit, see [37] for details. The first three terms in (6) can be referred to as double spin-flip, spin-flip hopping, and single spin-flip, the latter being a descendant of the cubic term (2). As in the $1/S$ expansion, this is the only

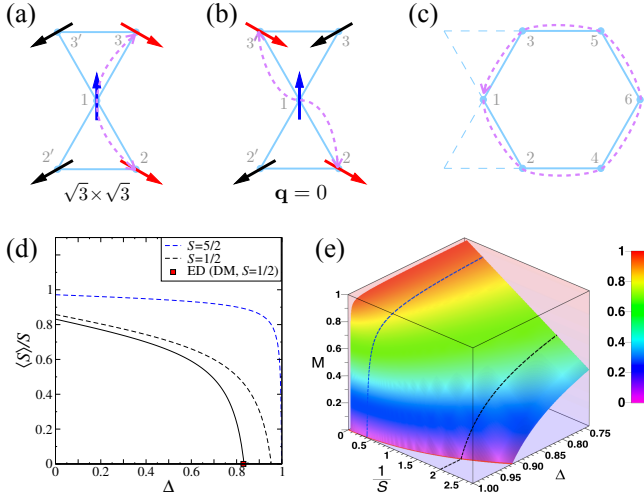


FIG. 3: (Color online) (a) and (b): schematics of the symmetry related processes of the 4th order. (c) Topologically non-trivial path of the 7th order. (d) Magnetization $M = \langle S \rangle / S$ vs Δ in linear SWT for $S = 1/2$ and $S = 5/2$, dashed lines. Solid line, a sketch of $M(\Delta)$ for the case of DM interaction. (e) Linear SWT result for $M(S, \Delta)$.

term which is sensitive to the 120° pattern and, therefore, is the key to the selection of the ground state.

Since every term in the energy expansion corresponds to a finite cluster of spins coupled by perturbations in (6) and since the classical ground state is a vacuum for spin flips, contributions that are relevant to lifting the ground-state degeneracy must begin and end with a double spin-flip and must also contain a pair of single spin-flips. The first process of such kind appears in the fourth order, an example given by the operator sequence $\hat{V}_1^{12} \rightarrow \hat{V}_3^{13} \rightarrow \hat{V}_3^{12} \rightarrow \hat{V}_1^{13}$ shown in Fig. 3(a). The respective energy shift depends on the mutual orientation of \mathbf{S}_2 and \mathbf{S}_3 because $\delta E^{(4)} \propto \sin \theta_{12} \sin \theta_{13}$. However, an obvious symmetry leaves the degeneracy intact at this order of expansion, because for any coupling between \mathbf{S}_2 and \mathbf{S}_3 there is a “mirror” process that couples identically \mathbf{S}_2 with $\mathbf{S}_{3'}$, see Fig. 3(b), providing the same energy gain to both the $\sqrt{3} \times \sqrt{3}$ and the $\mathbf{q} = 0$ states.

Generalizing this trend, we conclude that the degeneracy-lifting terms must correspond to linked clusters of a non-trivial topology, with the smallest cluster consisting of a hexagon loop and generated by the seventh-order process depicted in Fig. 3(c). One example of the operator sequence is given by $\hat{V}_1^{24} \rightarrow \hat{V}_3^{21} \rightarrow \hat{V}_3^{13} \rightarrow \hat{V}_1^{12} \rightarrow \hat{V}_1^{56} \rightarrow \hat{V}_1^{46} \rightarrow \hat{V}_1^{35}$ and contains five double-flips and two single-flips. This type of processes yields the only relevant seventh-order contribution at $\Delta = 1/2$, for which the amplitude A_- of the spin-flip hopping \hat{V}_2 (6) vanishes together with the rest of the degeneracy-lifting terms. The energy correction at $\Delta = 1/2$ corresponds to an effective antiferromagnetic coupling between the second-neighbor spins \mathbf{S}_2 and \mathbf{S}_3 , $\delta E^{(7)} \sim + \sin \theta_{12} \sin \theta_{13}$ [37],

favoring the $\mathbf{q} = 0$ state.

Moreover, one can show that for $\Delta < 1/2$ all relevant seventh-order processes have the same sign and also favor the $\mathbf{q} = 0$ state. For $\Delta > 1/2$, some of the terms switch sign. This implies that the transition to the $\sqrt{3} \times \sqrt{3}$ state can take place only at some $\Delta_c > 1/2$, in agreement with the the non-linear SWT result $\Delta_c \approx 0.72$.

There are close parallels between the non-linear SWT and the real-space approach. Although the degeneracy-lifting contribution in the RSPT is of the seventh order, it is still of the second order in cubic terms, same as in the non-linear SWT (4). More importantly, the high order of the relevant perturbation processes explains the smallness of the quantum ObD effect. Essentially, the RSPT is an expansion in $1/z$, where z is the coordination number, which gives the right order-of-magnitude estimate for the seventh-order effect $\delta E \sim 10^{-4} J$. A more careful calculation using the actual perturbation terms in (6) and combinatorial factors of different processes of seventh order gives a similar answer [37].

Phase diagram.—We now construct the phase diagram of the XXZ KGAFM (1) as a function of anisotropy Δ and spin S . For that, we calculate the ordered moment within the harmonic SWT approximation, $\langle S \rangle = S - \langle a_i^\dagger a_i \rangle$, to map out the extent of the magnetically ordered state. Because of the degeneracy of classical 120° states, harmonic spin-wave spectrum is identical in all of them and yields the same result. Here we simply estimate stability of the Néel order with respect to the “diagonal” quantum fluctuation for a given state. While this analysis completely neglects the “off-diagonal” tunneling within the manifold, such processes should be exponentially suppressed for larger spins [47].

Figure 3(d) shows magnetization $M = \langle S \rangle / S$ vs Δ for two representative values of the spin. Néel state is stabilized already at rather small $1 - \Delta'_c \approx 0.05$ for $S = 1/2$ and $1 - \Delta'_c \approx 0.002$ for $S = 5/2$. Considering spin S as a continuous variable, we plot $M(S, \Delta)$ in Fig. 3(e) where dashed lines are the same as in Fig. 3(d) and the color is for the magnitude of M . The $M = 0$ curve is the Néel order phase boundary in the S – Δ plane, see also Fig. 4(a). A simple algebra yields an asymptotic expression for it, $1 - \Delta'_c \approx (96S^2)^{-1}$, which agrees exceedingly well with the results of numerical integration [37].

In Fig. 3(d) we also sketch results of the Exact Diagonalization (ED) for $S = 1/2$ KGAFM with the out-of-plane DM term [33], which selects $\mathbf{q} = 0$ ground state but yields harmonic Hamiltonian identical to the XXZ case with rescaling $1 - \Delta \Leftrightarrow \sqrt{3}D_z$ [31, 36, 48]. Since the DM term suppresses tunneling processes within the manifold, it is reasonable to compare ED with SWT results to evaluate the accuracy of the SWT Néel order boundary. For the latter, one can see a qualitative agreement with ED and a quantitative exaggeration of the extent of the ordered phase, expected for the SWT approach.

We now combine our SWT results in Fig. 4(a), which

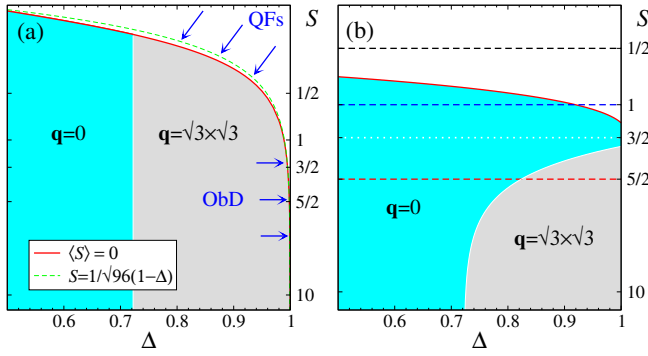


FIG. 4: (Color online) (a) S – Δ phase diagram, S is on the logarithmic scale. Solid line is the Neél order boundary $\langle S \rangle = 0$ from the linear SWT, dashed line is its asymptotic approximation. Vertical boundary between $\mathbf{q}=0$ and $\sqrt{3} \times \sqrt{3}$ states is from the non-linear SWT. (b) Tentative S – Δ phase diagram. Suppression of magnetic order by quantum fluctuations (QFs) and quantum ObD near the Heisenberg limit are suggested. Horizontal lines are cuts for different values of the spin.

shows the S – Δ phase diagram. The solid line is the linear SWT result for the Neél order boundary $\langle S \rangle = 0$, see also Fig. 3(e), and the dashed line is its asymptotic approximation mentioned above. As we discussed, the harmonic treatment gives a good qualitative idea for the phase boundary between magnetically ordered and disordered phases, but *does not* specify which of the 120° Neél states is chosen. We infer this information from the non-linear SWT results in Fig. 2 and complete our perturbative S – Δ phase diagram by adding the boundary between $\mathbf{q}=0$ and $\sqrt{3} \times \sqrt{3}$ states.

There are two trends that are not included in this phase diagram and are beyond the methods used in the current work. The non-linear SWT approach is a perturbative treatment of the quantum ObD effect, which fails in the vicinity of the Heisenberg limit. However, it is known that quantum ObD should extend Neél-ordered region of the phase diagram to the $\Delta=1$ axis for larger spin values. It has been argued by the self-consistent version of SWT [4] that the $\sqrt{3} \times \sqrt{3}$ is the ground state of the Heisenberg KGAFM for $S \gg 1$.

The other trend is the suppression of the Neél order by quantum fluctuations for smaller spins, leading to the growth of the non-magnetic region of the phase diagram. As was argued recently by several groups using numerical approaches [49–51], the $S=1/2$ XXZ KGAFM remains in a spin-liquid state for the entire range of $\Delta \leq 1$. Our results for $S=1/2$ case in Fig. 4(a) are, therefore, inadequate, most likely because of the neglect of the tunneling between different states in 120° manifold.

In order to capture some of these trends we modify the mean-field condition $\langle S \rangle = 0$ used above by including the self-consistently renormalized spin-wave dispersion of the “flat mode” for the Heisenberg limit from [4]. While this is not an entirely rigorous procedure, it should provide a

reasonable estimate on the extent of the region of stability due to quantum ObD for $\Delta=1$. The resulting values for the “critical” S_c , above which the system orders magnetically, come out as $S_c^{\mathbf{q}=0} \approx 0.17$ and $S_c^{\sqrt{3} \times \sqrt{3}} \approx 0.18$. While, obviously, this is another case of quantitative exaggeration of the extent of the ordered phase by an SWT approach, this estimate makes it extremely unlikely that the Heisenberg KGAFM with $S \gtrsim 1$ will be magnetically disordered. In fact, recent numerical work [17] has indicated that the Heisenberg KGAFMs with $S \geq 3/2$ all order in a $\sqrt{3} \times \sqrt{3}$ configuration.

Combining these trends, we propose a tentative S – Δ phase diagram of the nearest-neighbor XXZ KGAFM model in Fig. 4(b). In the Heisenberg limit, for larger values of spin the ground state is $\sqrt{3} \times \sqrt{3}$ state, which switches to $\mathbf{q}=0$ upon reducing Δ . For $S=1$ the same trajectory begins with the magnetically disordered state and the system enters directly into the $\mathbf{q}=0$ state. As shown by the recent numerical results, $S=1/2$ remains quantum disordered for the entire range of Δ . Finally, there may, or may not, exist an intermediate value of spin for which Heisenberg limit is already in the $\mathbf{q}=0$ domain and no transition occurs versus Δ . While predictions of this work are firm for the larger values of spin, the ultimate answer on the exact sequence of phases for smaller spins should be sought via numerical approaches.

Conclusions.—By advancing the non-linear $1/S$ expansion and the real-space perturbation theory we investigated quantum order-by-disorder selection of the ground state of the nearest-neighbor XXZ antiferromagnet on the kagomé lattice. We demonstrated that the order selection is generated by topologically non-trivial tunneling processes, presented a strong evidence of the rare case of quantum and thermal fluctuations favoring different ground states, proposed a tentative S – Δ phase diagram of the model, and suggested further studies.

We acknowledge useful discussions with C. Batista, F. Becca, A. V. Chubukov, G. Jackeli, A. Läuchli, R. Moessner, N. Perkins, S. Parameswaran, H. Tsunetsugu, and S. R. White. Work by A. L. C. was supported by the U.S. Department of Energy, Office of Science, Basic Energy Sciences under Award # DE-FG02-04ER46174. A. L. C. would like to thank Aspen Center for Physics, where part of this work was done, for hospitality. The work at Aspen was supported in part by NSF Grant No. PHYS-1066293.

-
- [1] C. Zeng and V. Elser, Phys. Rev. B **42**, 8436 (1990).
 - [2] A. B. Harris, C. Kallin, and A. J. Berlinsky, Phys. Rev. B **45**, 2899 (1992).
 - [3] J. T. Chalker, P. C. W. Holdsworth, and E. F. Shender, Phys. Rev. Lett. **68**, 855 (1992).
 - [4] A. Chubukov, Phys. Rev. Lett. **69**, 832 (1992); J. Appl. Phys. **73**, 5639 (1993).
 - [5] S. Sachdev, Phys. Rev. B **45**, 12377 (1992).

- [6] J. T. Chalker and J. F. G. Eastmond, Phys. Rev. B **46**, 14201 (1992).
- [7] R. R. P. Singh and D. A. Huse, Phys. Rev. Lett. **68**, 1766 (1992).
- [8] P. Lecheminant, B. Bernu, C. Lhuillier, L. Pierre, and P. Sindzingre, Phys. Rev. B **56**, 2521 (1997).
- [9] M. Mambrini and F. Mila, Eur. Phys. J. B **17**, 651 (2000).
- [10] P. Nikolic and T. Senthil, Phys. Rev. B **68**, 214415 (2003).
- [11] R. R. P. Singh and D. A. Huse, Phys. Rev. B **76**, 180407(R) (2007).
- [12] J. S. Helton, K. Matan, M. P. Shores, E. A. Nytko, B. M. Bartlett, Y. Yoshida, Y. Takano, A. Suslov, Y. Qiu, J.-H. Chung, D. G. Nocera, and Y. S. Lee, Phys. Rev. Lett. **98**, 107204 (2007).
- [13] T.-H. Han, J. S. Helton, S. Chu, D. G. Nocera, J. A. Rodriguez-Rivera, C. Broholm, and Y. S. Lee, Nature (London) **492**, 406 (2012).
- [14] K. Matan, T. Ono, Y. Fukumoto, T. J. Sato, J. Yamaura, M. Yano, K. Morita, and H. Tanaka, Nature Phys. **6**, 865 (2010).
- [15] K. Matan, Y. Nambu, Y. Zhao, T. J. Sato, Y. Fukumoto, T. Ono, H. Tanaka, C. Broholm, A. Podlesnyak, and G. Ehlers, Phys. Rev. B **89**, 024414 (2014).
- [16] S. Yan, D. A. Huse, and S. R. White, Science **332**, 1173 (2011).
- [17] O. Götze, D. J. J. Farnell, R. F. Bishop, P. H. Y. Li, and J. Richter, Phys. Rev. B **84**, 224428 (2011).
- [18] L. Balents, Nature (London) **464**, 199 (2010).
- [19] Y. Iqbal, F. Becca, S. Sorella, and D. Poilblanc, Phys. Rev. B **87**, 060405 (2013).
- [20] H. J. Changlani and A. M. Läuchli, arXiv:1406.4767 [cond-mat.str-el].
- [21] T. Liu, W. Li, A. Weichselbaum, J. von Delft, and G. Su, arXiv:1406.5905 [cond-mat.str-el].
- [22] S. Nishimoto and M. Nakamura, arXiv:1409.5870 [cond-mat.str-el].
- [23] I. Rousochatzakis, Y. Wan, Oleg Tchernyshyov, and F. Mila, Phys. Rev. B **90**, 100406(R) (2014).
- [24] Z. Hao and O. Tchernyshyov, Phys. Rev. B **81**, 214445 (2010).
- [25] Y. Wan and O. Tchernyshyov, Phys. Rev. B **87**, 104408 (2013).
- [26] M. Taillefumier, J. Robert, C. L. Henley, R. Moessner, and B. Canals, arXiv:1403.7903 [cond-mat.str-el].
- [27] A. Zorko, S. Nellutla, J. van Tol, L. C. Brunel, F. Bert, F. Duc, J.-C. Trombe, M. A. de Vries, A. Harrison, and P. Mendels, Phys. Rev. Lett. **101**, 026405 (2008).
- [28] A. Zorko, F. Bert, A. Ozarowski, J. van Tol, D. Boldrin, A. S. Wills, and P. Mendels, Phys. Rev. B **88**, 144419 (2013).
- [29] K. Matan, D. Grohol, D. G. Nocera, T. Yildirim, A. B. Harris, S. H. Lee, S. E. Nagler, and Y. S. Lee, Phys. Rev. Lett. **96**, 247201 (2006).
- [30] H. Yoshida, Y. Michiue, E. Takayama-Muromachi, and M. Isobe, J. Mater. Chem. **22**, 18793 (2012).
- [31] T. Yildirim and A. B. Harris, Phys. Rev. B **73**, 214446 (2006).
- [32] M. Elhajal, B. Canals, and C. Lacroix, Phys. Rev. B **66**, 014422 (2002).
- [33] O. Cépas, C. M. Fong, P. W. Leung, and C. Lhuillier, Phys. Rev. B **78**, 140405 (2008).
- [34] L. Messio, O. Cépas, and C. Lhuillier, Phys. Rev. B **81**, 064428 (2010).
- [35] Y. Huh, L. Fritz, and S. Sachdev, Phys. Rev. B **81**, 144432 (2010).
- [36] We note that there exist a close similarity of the harmonic part of the XXZ model and the kagomé Hamiltonian with the out-of-plane DM interaction D_z . However, in the latter case the ground state is selected on a classical level. In that sense, XXZ anisotropy is a much lighter perturbation as it does not lift the macroscopic degeneracy between the manifold of 120° states and allows to study a purely quantum ObD mechanism.
- [37] See Supplemental Material for details of theoretical calculations for the kagomé antiferromagnet.
- [38] J. N. Reimers and A. J. Berlinsky, Phys. Rev. B **48**, 9539 (1993).
- [39] C. L. Henley, Phys. Rev. B **80**, 180401(R) (2009).
- [40] D. A. Huse and A. D. Rutenberg, Phys. Rev. B **45**, 7536(R) (1992).
- [41] S. E. Korshunov, Phys. Rev. B **65**, 054416 (2002).
- [42] M. S. Rzchowski, Phys. Rev. B **55**, 11745 (1997).
- [43] M. W. Long, J. Phys.: Condens. Matter **1**, 2857 (1989).
- [44] M. T. Heinilä and A. S. Oja, Phys. Rev. B **48**, 7227 (1993).
- [45] B. Canals and M. E. Zhitomirsky, J. Phys.: Condens. Matter **16**, S759 (2004).
- [46] D. L. Bergman, R. Shindou, G. A. Fiete, and L. Balents, Phys. Rev. B **75**, 094403 (2007).
- [47] J. von Delft and C. L. Henley, Phys. Rev. B **48**, 965 (1993).
- [48] R. Ballou, B. Canals, M. Elhajal, C. Lacroix, and A. Wills, J. Magn. Magn. Mat. **262**, 465 (2003).
- [49] A. M. Läuchli, private communication.
- [50] S. R. White, unpublished.
- [51] Y.-C. He and Y. Chen, arXiv:1407.2740 [cond-mat.str-el].

Quantum Selection of Order in an XXZ Antiferromagnet on a Kagomé Lattice: Supplemental Material

A. L. Chernyshev¹ and M. E. Zhitomirsky²

¹*Department of Physics and Astronomy, University of California, Irvine, California 92697, USA*

²*Service de Physique Statistique, Magnétisme et Supraconductivité,*

UMR-E9001 CEA-INAC/UJF, 17 rue des Martyrs, 38054 Grenoble Cedex 9, France

(Dated: September 24, 2014)

SPIN-WAVE THEORY

Spin Hamiltonian

We consider a kagomé-lattice antiferromagnet with anisotropic XXZ exchange interactions

$$\hat{\mathcal{H}} = J \sum_{\langle ij \rangle} \left(S_i^x S_j^x + S_i^y S_j^y + \Delta S_i^z S_j^z \right), \quad (7)$$

where summation is over bonds, i, j numerate the sites of the kagomé lattice, and anisotropy is assumed to be of the easy-plane type, $0 \leq \Delta \leq 1$. In a semiclassically ordered state spins of the kagomé-lattice antiferromagnet form a coplanar 120° structure in the xy plane. Transforming to a rotating local basis we can rewrite (7) as

$$\begin{aligned} \hat{\mathcal{H}} = & J \sum_{\langle ij \rangle} \left(\Delta S_i^y S_j^y + \cos \theta_{ij} (S_i^x S_j^x + S_i^z S_j^z) \right. \\ & \left. + \sin \theta_{ij} (S_i^z S_j^x - S_i^x S_j^z) \right) = J \sum_{\langle ij \rangle} \mathbf{S}_i \otimes \mathbf{S}_j, \quad (8) \end{aligned}$$

where $\theta_{ij} = \theta_i - \theta_j$ is an angle between two neighboring spins and we have introduced “matrix” product of spins \otimes as a shorthand notation.

We choose the unit cell of the kagomé lattice as an up-triangle with three atoms in the positions

$$\boldsymbol{\rho}_1 = (0, 0), \quad \boldsymbol{\rho}_2 = \left(-\frac{1}{4}, \frac{\sqrt{3}}{4} \right), \quad \boldsymbol{\rho}_3 = \left(-\frac{1}{2}, 0 \right). \quad (9)$$

All distances are given in units of $2a$ where a is the interatomic distance. The corresponding Bravais lattice is

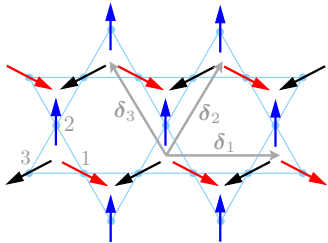


FIG. 5: Numbering of sites within the unit cell and primitive vectors of the kagomé lattice.

a triangular lattice with the primitive vectors

$$\boldsymbol{\delta}_1 = (1, 0), \quad \boldsymbol{\delta}_2 = \left(\frac{1}{2}, \frac{\sqrt{3}}{2} \right), \quad \boldsymbol{\delta}_3 = \boldsymbol{\delta}_2 - \boldsymbol{\delta}_1, \quad (10)$$

such that $\boldsymbol{\rho}_2 = \frac{1}{2}\boldsymbol{\delta}_3$ and $\boldsymbol{\rho}_3 = -\frac{1}{2}\boldsymbol{\delta}_1$, see Fig. 5. Then, changing the lattice sum to the sum over the unit cells and atomic index, $i \rightarrow \{\alpha, \ell\}$, with $\alpha = 1, 2, 3$ numerating atoms within the unit cell, Hamiltonian (8) becomes

$$\begin{aligned} \hat{\mathcal{H}} = & J \sum_{\ell} \mathbf{S}_{1,\ell} \otimes (\mathbf{S}_{2,\ell} + \mathbf{S}_{2,\ell-3}) \\ & + \mathbf{S}_{1,\ell} \otimes (\mathbf{S}_{3,\ell} + \mathbf{S}_{3,\ell+1}) + \mathbf{S}_{2,\ell} \otimes (\mathbf{S}_{3,\ell} + \mathbf{S}_{3,\ell+2}), \end{aligned} \quad (11)$$

where the product $\mathbf{S}_{\alpha,\ell} \otimes \mathbf{S}_{\alpha',\ell'}$ is according to (8), and $\ell \pm n \equiv \mathbf{R}_\ell \pm \boldsymbol{\delta}_n$ with the coordinate of the unit cell $\mathbf{R}_\ell = m_1\boldsymbol{\delta}_1 + m_2\boldsymbol{\delta}_2 + m_3\boldsymbol{\delta}_3$.

Linear spin-wave theory

Following the approach of Ref. [1], we introduce Holstein-Primakoff representation for spin operators in the local basis in (8) and (11) and, keeping only quadratic terms, obtain harmonic Hamiltonian for the three species of bosons, $a_{\alpha,\ell}(a_{\alpha,\ell}^\dagger)$. With the subsequent Fourier transformation of bosonic operators performed according to

$$a_{\alpha,\ell} = \frac{1}{\sqrt{N}} \sum_{\mathbf{k}} a_{\alpha,\mathbf{k}} e^{i\mathbf{k}\mathbf{r}_{\alpha,\ell}} \quad (12)$$

where $\mathbf{r}_{\alpha,\ell} = \boldsymbol{\rho}_\alpha + \mathbf{R}_\ell$ and N is the number of unit cells, we obtain linear SWT Hamiltonian

$$\begin{aligned} \hat{\mathcal{H}}_2 = & 2JS \sum_{\mathbf{k}, \alpha\beta} \left\{ \left[\delta_{\alpha,\beta} + \frac{(2\Delta - 1)}{4} \Lambda_{\alpha\beta}(\mathbf{k}) \right] a_{\alpha,\mathbf{k}}^\dagger a_{\beta,\mathbf{k}} \right. \\ & \left. - \frac{(2\Delta + 1)}{8} \Lambda_{\alpha\beta}(\mathbf{k}) (a_{\alpha,\mathbf{k}}^\dagger a_{\beta,-\mathbf{k}}^\dagger + \text{h.c.}) \right\}, \quad (13) \end{aligned}$$

where we introduce the matrix

$$\hat{\Lambda}_{\mathbf{k}} = \begin{pmatrix} 0 & c_3 & c_1 \\ c_3 & 0 & c_2 \\ c_1 & c_2 & 0 \end{pmatrix}, \quad (14)$$

and shorthand notations $c_n = \cos(q_n)$ with $q_n = \mathbf{k} \cdot \boldsymbol{\delta}_n/2$.

One can rewrite this Hamiltonian in the matrix form

$$\hat{\mathcal{H}}_2 = \sum_{\mathbf{k} > 0} \hat{X}_{\mathbf{k}}^\dagger \hat{\mathbf{H}}_{\mathbf{k}} \hat{X}_{\mathbf{k}} - 3JS, \quad (15)$$

with the vector operator

$$\hat{X}_{\mathbf{k}}^\dagger = (a_{1,\mathbf{k}}^\dagger, a_{2,\mathbf{k}}^\dagger, a_{3,\mathbf{k}}^\dagger, a_{1,-\mathbf{k}}, a_{2,-\mathbf{k}}, a_{3,-\mathbf{k}}) \quad (16)$$

and the 6×6 matrix $\hat{\mathbf{H}}_{\mathbf{k}}$

$$\hat{\mathbf{H}}_{\mathbf{k}} = 2JS \begin{pmatrix} \hat{\mathbf{A}}_{\mathbf{k}} & \hat{\mathbf{B}}_{\mathbf{k}} \\ \hat{\mathbf{B}}_{\mathbf{k}} & \hat{\mathbf{A}}_{\mathbf{k}} \end{pmatrix}, \quad (17)$$

where

$$\hat{\mathbf{A}}_{\mathbf{k}} = \hat{\mathbf{I}} + \frac{(2\Delta - 1)}{4} \hat{\mathbf{A}}_{\mathbf{k}}, \quad \hat{\mathbf{B}}_{\mathbf{k}} = -\frac{(2\Delta + 1)}{4} \hat{\mathbf{A}}_{\mathbf{k}}, \quad (18)$$

and $\hat{\mathbf{I}}$ being the identity matrix.

Because of an obvious commutativity of the matrices $\hat{\mathbf{A}}_{\mathbf{k}}$ and $\hat{\mathbf{B}}_{\mathbf{k}}$, their eigenvalues are straightforwardly related to the eigenvalues of $\hat{\mathbf{H}}_{\mathbf{k}}$, and, in turn, are determined by the eigenvalues of the matrix $\hat{\mathbf{A}}_{\mathbf{k}}$, so that the spin-wave excitation energies are

$$\varepsilon_{\nu,\mathbf{k}} = 2JS \sqrt{A_{\nu,\mathbf{k}}^2 - B_{\nu,\mathbf{k}}^2} = 2JS \omega_{\nu,\mathbf{k}}, \quad (19)$$

with

$$A_{\nu,\mathbf{k}} = 1 + \frac{(2\Delta - 1)}{4} \lambda_{\nu,\mathbf{k}}, \quad B_{\nu,\mathbf{k}} = -\frac{(2\Delta + 1)}{4} \lambda_{\nu,\mathbf{k}}. \quad (20)$$

Thus, the problem of diagonalization of $\hat{\mathcal{H}}_2$ in (13) is reduced to the eigenvalue problem of $\hat{\mathbf{A}}_{\mathbf{k}}$ (14). From the characteristic equation for the matrix $\hat{\mathbf{A}}_{\mathbf{k}}$ one finds

$$|\hat{\mathbf{A}}_{\mathbf{k}} - \lambda| = (\lambda + 1)(\lambda^2 - \lambda - 2\gamma_{\mathbf{k}}) = 0, \quad (21)$$

where $\gamma_{\mathbf{k}} \equiv c_1 c_2 c_3$ is introduced and factorization is performed with the help of a useful identity

$$c_1^2 + c_2^2 + c_3^2 = 1 + 2c_1 c_2 c_3.$$

Thus, the λ -eigenvalues are

$$\lambda_1 = -1, \quad \lambda_{2(3),\mathbf{k}} = \frac{1}{2} \left(1 \pm \sqrt{1 + 8\gamma_{\mathbf{k}}} \right), \quad (22)$$

and one of the spin-wave excitations is completely dispersionless (“flat mode”)

$$\varepsilon_{1,\mathbf{k}} = 2JS \sqrt{3(1 - \Delta)/2}, \quad (23)$$

whereas the other two are given by

$$\varepsilon_{2(3),\mathbf{k}} = 2JS \sqrt{1 - \Delta\gamma_{\mathbf{k}} - (1 - \Delta)(1 \pm \sqrt{1 + 8\gamma_{\mathbf{k}}})/4}.$$

In the Heisenberg limit, $\Delta = 1$, the flat mode has zero energy, while the other two modes are degenerate

$$\varepsilon_{2(3),\mathbf{k}} = 2JS \sqrt{1 - \gamma_{\mathbf{k}}}. \quad (24)$$

Two-step diagonalization

Following Harris *et al.* [1], the diagonalization of $\hat{\mathbf{A}}_{\mathbf{k}}$ implies a two-step diagonalization procedure of $\hat{\mathcal{H}}_2$ in (13). The eigenvectors $\mathbf{w}_\nu = (w_{\nu,1}(\mathbf{k}), w_{\nu,2}(\mathbf{k}), w_{\nu,3}(\mathbf{k}))$

$$\hat{\mathbf{A}}_{\mathbf{k}} \mathbf{w}_\nu = \lambda_{\nu,\mathbf{k}} \mathbf{w}_\nu \quad (25)$$

are given explicitly by

$$\mathbf{w}_\nu(\mathbf{k}) = \frac{1}{r_\nu} \begin{pmatrix} c_1 c_2 + \lambda_{\nu} c_3 \\ \lambda_{\nu}^2 - c_1^2 \\ c_1 c_3 + \lambda_{\nu} c_2 \end{pmatrix}, \quad (26)$$

with $r_\nu = \sqrt{(c_1 c_2 + \lambda_{\nu} c_3)^2 + (\lambda_{\nu}^2 - c_1^2)^2 + (c_1 c_3 + \lambda_{\nu} c_2)^2}$.

These eigenvectors define a *unitary* transformation from the Holstein-Primakoff bosons to the new ones

$$d_{\nu,\mathbf{k}} = \sum_{\alpha} w_{\nu,\alpha}(\mathbf{k}) a_{\alpha,\mathbf{k}}, \quad a_{\alpha,\mathbf{k}} = \sum_{\nu} w_{\nu,\alpha}(\mathbf{k}) d_{\nu,\mathbf{k}}, \quad (27)$$

such that $\hat{\mathcal{H}}_2$ in (13) is partially diagonalized

$$\hat{\mathcal{H}}_2 = 2JS \sum_{\nu,\mathbf{k}} \left(A_{\nu,\mathbf{k}} d_{\nu,\mathbf{k}}^\dagger d_{\nu,\mathbf{k}} - \frac{B_{\nu,\mathbf{k}}}{2} \left(d_{\nu,\mathbf{k}}^\dagger d_{\nu,-\mathbf{k}}^\dagger + \text{h.c.} \right) \right). \quad (28)$$

Finally, we apply the canonical Bogolyubov transformation for each individual species of d -boson

$$d_{\nu,\mathbf{k}} = u_{\nu,\mathbf{k}} b_{\nu,\mathbf{k}} + v_{\nu,\mathbf{k}} b_{\nu,-\mathbf{k}}^\dagger, \quad (29)$$

with $u_{\nu,\mathbf{k}}^2 - v_{\nu,\mathbf{k}}^2 = 1$ and

$$v_{\nu,\mathbf{k}}^2 = \frac{1}{2} \left(\frac{A_{\nu,\mathbf{k}}}{\omega_{\nu,\mathbf{k}}} - 1 \right), \quad 2u_{\nu,\mathbf{k}} v_{\nu,\mathbf{k}} = \frac{B_{\nu,\mathbf{k}}}{\omega_{\nu,\mathbf{k}}}, \quad (30)$$

to diagonalize (28) completely with the eigenvalues (19). The importance of this two-step procedure will be apparent in the discussions of the non-linear terms.

Cubic terms

The non-linear $S_i^x S_j^z$ terms in (8) are the only ones that are able to distinguish between different 120° spin configurations by virtue of containing $\sin \theta_{ij} = \pm \sqrt{3}/2$ for the clockwise or counterclockwise spin rotation. In the bosonic representation they yield cubic terms

$$\hat{\mathcal{H}}_3 = J \sqrt{\frac{S}{2}} \sum_{i,j} \sin \theta_{ij} (a_i^\dagger a_j^\dagger a_j + \text{h.c.}), \quad (31)$$

where $\theta_{ij} = \theta_i - \theta_j$ is an angle between two neighboring spins as before. This results into anharmonic interaction of spin waves with the amplitudes which are *different*

for different ordered structures. Below we obtain cubic vertices for the $\mathbf{q}=0$ and $\sqrt{3} \times \sqrt{3}$ states.

For the $\mathbf{q}=0$ pattern (31) can be rewritten as

$$\hat{\mathcal{H}}_3 = -J\sqrt{\frac{3S}{2N}} \sum_{\alpha\beta, \mathbf{k}, \mathbf{q}} \epsilon^{\alpha\beta\gamma} \cos(q_{\beta\alpha}) a_{\alpha, \mathbf{q}}^\dagger a_{\beta, \mathbf{k}}^\dagger a_{\beta, \mathbf{p}} + \text{h.c.}, \quad (32)$$

where $\epsilon^{\alpha\beta\gamma}$ is the Levi-Civita antisymmetric tensor, $\mathbf{p} = \mathbf{k} + \mathbf{q}$, and shorthand notations $q_{\beta\alpha} = \mathbf{q}\rho_{\beta\alpha}$ and $\rho_{\beta\alpha} = \boldsymbol{\rho}_\beta - \boldsymbol{\rho}_\alpha$ are introduced.

Next we perform the two-step transformation. The unitary transformation (27) yields

$$\hat{\mathcal{H}}_3 = -J\sqrt{\frac{3S}{2N}} \sum_{\mathbf{k}, \mathbf{q}} \sum_{\nu\mu\eta} F_{\mathbf{q}\mathbf{k}\mathbf{p}}^{\nu\mu\eta} d_{\nu, \mathbf{q}}^\dagger d_{\mu, \mathbf{k}}^\dagger d_{\eta, \mathbf{p}} + \text{h.c.}, \quad (33)$$

with the amplitude

$$F_{\mathbf{q}\mathbf{k}\mathbf{p}}^{\nu\mu\eta} = \sum_{\alpha\beta} \epsilon^{\alpha\beta\gamma} \cos(q_{\beta\alpha}) w_{\nu, \alpha}(\mathbf{q}) w_{\mu, \beta}(\mathbf{k}) w_{\eta, \beta}(\mathbf{p}). \quad (34)$$

The subsequent Bogolyubov transformation (29) generates the “source”, $b^\dagger b^\dagger b^\dagger$, and the “decay”, $b^\dagger b^\dagger b$, terms. For the $1/S$ expansion of the groundstate energy we need only the source terms

$$\hat{\mathcal{H}}_3 = \frac{1}{3!} \frac{1}{\sqrt{N}} \sum_{\mathbf{k}+\mathbf{p}+\mathbf{q}=0} V_{\mathbf{q}\mathbf{k}\mathbf{p}}^{\nu\mu\eta} b_{\nu, \mathbf{q}}^\dagger b_{\mu, \mathbf{k}}^\dagger b_{\eta, \mathbf{p}}^\dagger + \text{h.c.}, \quad (35)$$

with the vertex

$$V_{\mathbf{q}\mathbf{k}\mathbf{p}}^{\nu\mu\eta} = -J\sqrt{\frac{3S}{2}} \tilde{V}_{\mathbf{q}\mathbf{k}\mathbf{p}}^{\nu\mu\eta}, \quad (36)$$

and the fully symmetrized dimensionless vertex given by

$$\begin{aligned} \tilde{V}_{\mathbf{q}\mathbf{k}\mathbf{p}}^{\nu\mu\eta} = & F_{\mathbf{q}\mathbf{k}\mathbf{p}}^{\nu\mu\eta} (u_{\nu\mathbf{q}} + v_{\nu\mathbf{q}}) (u_{\mu\mathbf{k}} v_{\eta\mathbf{p}} + v_{\mu\mathbf{k}} u_{\eta\mathbf{p}}) \\ & + F_{\mathbf{k}\mathbf{p}\mathbf{q}}^{\mu\eta\nu} (u_{\mu\mathbf{k}} + v_{\mu\mathbf{k}}) (u_{\nu\mathbf{p}} v_{\eta\mathbf{q}} + v_{\nu\mathbf{p}} u_{\eta\mathbf{q}}) \\ & + F_{\mathbf{p}\mathbf{q}\mathbf{k}}^{\eta\nu\mu} (u_{\eta\mathbf{p}} + v_{\eta\mathbf{p}}) (u_{\nu\mathbf{q}} v_{\mu\mathbf{k}} + v_{\nu\mathbf{q}} u_{\mu\mathbf{k}}), \end{aligned} \quad (37)$$

for deriving which we have used the symmetry property $F_{\mathbf{q}\mathbf{k}\mathbf{p}}^{\nu\mu\eta} = F_{\mathbf{q}\mathbf{p}\mathbf{k}}^{\nu\eta\mu}$.

Repeating the same calculation for the $\sqrt{3} \times \sqrt{3}$ state results in the identical expression of the cubic spin-wave Hamiltonian (35) and corresponding vertices (36) and (37), but with different amplitude $F_{\mathbf{q}\mathbf{k}\mathbf{p}}^{\nu\mu\eta}$

$$F_{\mathbf{q}\mathbf{k}\mathbf{p}}^{\nu\mu\eta} = i \sum_{\alpha\beta} \epsilon^{\alpha\beta\gamma} \sin(q_{\beta\alpha}) w_{\nu, \alpha}(\mathbf{q}) w_{\mu, \beta}(\mathbf{k}) w_{\eta, \beta}(\mathbf{p}). \quad (38)$$

The second-order correction to the ground state energy due to cubic terms is given by

$$\delta E^{(3)} = -\frac{1}{6N} \sum_{\nu\mu\eta} \sum_{\mathbf{q}, \mathbf{k}} \frac{|V_{\mathbf{q}, \mathbf{k}, -\mathbf{k}-\mathbf{q}}^{\nu\mu\eta}|^2}{\varepsilon_{\nu, \mathbf{q}} + \varepsilon_{\mu, \mathbf{k}} + \varepsilon_{\eta, -\mathbf{k}-\mathbf{q}}}, \quad (39)$$

This energy is per unit cell of 3 spins. Summation over magnon branches gives 27 individual contributions of which only 10 are independent.

Ordered magnetic moment

Within the linear SWT, magnetic moment on a site that belongs to the sublattice α is reduced by zero-point fluctuations

$$\langle S \rangle_\alpha = S - \langle a_{\alpha, i}^\dagger a_{\alpha, i} \rangle. \quad (40)$$

Converting from a_α to d_μ and then to b_μ operators using unitary (27) and then Bogolyubov (29) transformations one arrives to

$$\langle S \rangle_\alpha = S - \frac{1}{N} \sum_{\mu, \mathbf{k}} w_{\mu, \alpha}^2(\mathbf{k}) v_{\mu\mathbf{k}}^2. \quad (41)$$

Since all three sublattices are equivalent, symmetrization of (41) gives

$$\langle S \rangle = S - \frac{1}{3N} \sum_{\mu, \mathbf{k}} v_{\mu\mathbf{k}}^2, \quad (42)$$

with $v_{\mu\mathbf{k}}^2$ from (30). Since Bogolyubov parameters are implicit functions of anisotropy Δ , calculations of the magnetization $M = \langle S \rangle / S$ and the $\langle S \rangle = 0$ Neél order boundary in the $S-\Delta$ plane can be performed taking the 2D integrals in (42) numerically for the range of $0 < \Delta < 1$.

Quantum suppression of the ordered moment vs anisotropy Δ is shown in Fig. 6(a) for two values of spin. Quantum correction diverges for $\Delta \rightarrow 1$ due to vanishing energy of the “flat mode,” suggesting a disordered state near the Heisenberg limit for all spins. The critical value $1 - \Delta_c \approx 0.047$ for $S = 1/2$ is also compared with the result for the Dzyaloshinskii-Moriya (DM) coupling $D_c = 0.1$ (with the proper rescaling $1 - \Delta \Leftrightarrow \sqrt{3}D$), found by Exact Diagonalization (ED) [2, 3].

Near the Heisenberg limit one can neglect non-divergent terms in the integrals in (42) and find an asymptotic expression for the Neél order boundary from

$$\langle S \rangle = 0 \approx S - \frac{1}{6} \frac{A_1}{\omega_1}, \quad (43)$$

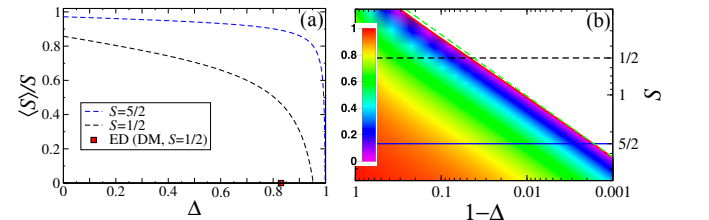


FIG. 6: (a) Linear SWT result for the magnetization $\langle S \rangle / S$ vs Δ for $S=1/2$ and $S=5/2$, dashed lines. Square is ED result for the case of $S=1/2$ with DM interaction. (b) Solid line is the $M=0$ Neél order phase boundary in the $S-\Delta$ plane on the log-log scale, dashed line is the asymptotic approximation for it; color is for the magnitude of M .

where $A_1 = 3/4$, see (20), and $\omega_1 = \sqrt{3(1-\Delta)/2}$, see (23), leading to

$$1 - \Delta_c \approx \frac{1}{96S^2}, \quad (44)$$

which is shown in Fig. 6(b) together with the result of the numerical integration in (42).

In the same spirit, we attempt to capture the non-perturbative effects of order-by-disorder mechanism at the Heisenberg limit by using the self-consistently renormalized spin-wave dispersion of the “flat mode” from [4] instead of the dispersionless mode in (23) for the calculation of the mean-field Néel order boundary $\langle S \rangle = 0$ from (42). This procedure should provide a reasonable estimate on the extent of the region of stability due to quantum order-by-disorder for $\Delta = 1$. In Ref. [4], the renormalized dispersion of the “flat mode” is

$$\tilde{\varepsilon}_{1,\mathbf{k}} = 2JS^{2/3}C_{SW}\sqrt{2}\omega_{2,\mathbf{k}}, \quad (45)$$

where $\omega_{2,\mathbf{k}} = \sqrt{1 - \gamma_{\mathbf{k}}}$ and the constant C_{SW} is defined numerically for two ordered phases: $C_{SW}^{\sqrt{3} \times \sqrt{3}} \approx 0.40$ and $C_{SW}^{\mathbf{q}=0} \approx 0.42$.

Again, neglecting the non-divergent terms in (42) reduces $\langle S \rangle = 0$ to

$$\langle S \rangle = 0 \approx S - \frac{1}{6N} \sum_{\mathbf{k}} \frac{2JSA_1}{\tilde{\varepsilon}_{1,\mathbf{k}}}, \quad (46)$$

which gives

$$S_c \approx \left(\frac{c_0}{8\sqrt{2}C_{SW}} \right)^{3/2}, \quad (47)$$

where $c_0 = \sum_{\mathbf{k}} 1/\sqrt{1 - \gamma_{\mathbf{k}}} = 1.4296$. The resulting values for the “critical” S_c come out as $S_c^{\mathbf{q}=0} \approx 0.17$ and $S_c^{\sqrt{3} \times \sqrt{3}} \approx 0.18$. Observe that $S_c^{\mathbf{q}=0} < S_c^{\sqrt{3} \times \sqrt{3}}$. While SWT approach clearly exaggerates the extent of the ordered phase, this estimate makes it extremely unlikely that the Heisenberg KGAFM with $S \gtrsim 1$ will be magnetically disordered.

REAL-SPACE PERTURBATION THEORY FOR KAGOMÉ ANTIFERROMAGNET

We develop a real-space perturbation expansion around the manifold of classical ground states [5–8] to determine the ordering pattern in the XXZ kagomé-lattice antiferromagnet. By analyzing perturbative terms of various order we suggest a real-space hierarchy of effective couplings that are responsible for the groundstate selection and give a simple qualitative explanation of the stability of the $\mathbf{q} = 0$ state for $\Delta = 1/2$.

Since the easy-plane anisotropy $\Delta < 1$ confines spins to xy plane, we consider only planar spin configurations.

Geometry of the kagomé lattice allows decomposition of the nearest-neighbor spin Hamiltonian (7) into the sum over triangles, see, e.g., [9], such that the classical Hamiltonian for an arbitrary planar state with $\mathbf{S}_i = (S_i^x, S_i^y, 0)$ can be written as

$$\hat{\mathcal{H}}_{\text{cl}} = \frac{J}{2} \sum_{\Delta} \mathbf{S}_{\Delta}^2 - J \sum_i \mathbf{S}_i^2. \quad (48)$$

Classical energy is minimized for $\mathbf{S}_{\Delta} = 0$, whereas the second term in (48) gives a constant $E_{\text{cl}}/N = -JS^2$. The constraint $\mathbf{S}_{\Delta} = 0$ forces spins on every triangle to form a 120° structure, but the translational pattern remains undetermined leading to a macroscopic number of degenerate ground states $W \approx 1.13471^N$ [$(\ln W)/N = 0.126377\dots$] [10, 11]. Degeneracy at the level of two triangles sharing a vertex is illustrated in Figs. 7(a) and (b) and correspond to $\sqrt{3} \times \sqrt{3}$ and $\mathbf{q} = 0$ states, respectively.

The local field acting on an individual spin is

$$\mathbf{h}_i = -\frac{\partial E_{\text{g.s.}}}{\partial \mathbf{S}_i} = 2JS\mathbf{n}_i \quad \text{with} \quad \mathbf{n}_i = \mathbf{S}_i/|\mathbf{S}_i|. \quad (49)$$

Because of the classical constraint only the last term in (48) contributes to $h = |\mathbf{h}_i| = 2JS$. The mean-field theory neglects fluctuations of h and does not lift the degeneracy, hence the need to include correlated fluctuations of spins. To construct perturbative expansion we use the Hamiltonian in the rotating local frame (8) and rearrange terms utilizing the value of the local field $h = 2JS$

$$\begin{aligned} \hat{\mathcal{H}} = h \sum_i \delta S_i^z + J \sum_{\langle ij \rangle} & \left(\Delta S_i^y S_j^y + S_i^x S_j^x \cos \theta_{ij} \right. \\ & \left. + \delta S_i^z \delta S_j^z \cos \theta_{ij} + \sin \theta_{ij} (S_i^z S_j^x - S_i^x S_j^z) \right), \end{aligned} \quad (50)$$

where the classical energy E_{cl} is neglected and we introduce $\delta S_i^z = S - S_i^z$. Note that for any 120° state $\cos \theta_{ij} \equiv -1/2$ whereas $\sin \theta_{ij} = \pm\sqrt{3}/2$.

The first term in (50) includes only on-site spin fluctuations and is chosen as the unperturbed Hamiltonian

$$\hat{\mathcal{H}}_0 = h \sum_i \delta S_i^z, \quad (51)$$

while the perturbation is naturally divided into four parts $\hat{V} = \sum_{i,j} (\hat{V}_1^{ij} + \hat{V}_2^{ij} + \hat{V}_3^{ij} + \hat{V}_4^{ij})$ with

$$\begin{aligned} \hat{V}_1^{ij} &= -\frac{J}{8} \left(\Delta + \frac{1}{2} \right) (S_i^+ S_j^+ + \text{H.c.}), \\ \hat{V}_2^{ij} &= \frac{J}{4} \left(\Delta - \frac{1}{2} \right) S_i^+ S_j^-, \\ \hat{V}_3^{ij} &= -\frac{J}{2} \sin \theta_{ij} \delta S_i^z (S_j^+ + S_j^-), \quad \hat{V}_4^{ij} = -\frac{J}{2} \delta S_i^z \delta S_j^z, \end{aligned} \quad (52)$$

where we have used $\cos \theta_{ij} = -1/2$ and left explicit $\sin \theta_{ij} = \pm\sqrt{3}/2$ in \hat{V}_3 . Since the ordering patterns differ by clockwise or counter-clockwise rotation of spins,

they can be distinguished only by the \hat{V}_3 operator, which, therefore, plays the key role in the groundstate selection. The first three terms in (52) can be referred to as the double spin-flip, spin-flip hopping, and single-flip, the latter is a descendant of the cubic term in (8).

The energy corrections generated by the expansion in \hat{V} can be obtained from the standard perturbation theory. One can formulate several simple rules, which help to identify contributions that are relevant to the ground-state selection:

- 1) Every member of the perturbation series must be represented by a linked cluster, ensuring that energy is extensive, $\delta E \sim N$, with each link corresponding to the action of one of the perturbation terms, \hat{V}_n^{ij} , acting on a specific lattice bond (i, j) . The total number of links is equal to the order of expansion. Several links on the same bond are allowed.
- 2) Any groundstate $|0\rangle$ from the classical 120° manifold is a vacuum for spin flips because all spins are fully oriented along their local fields, hence $\langle 0|\hat{V}|0\rangle = 0$. A simple inspection of \hat{V} in (52) shows that any term in the expansion must begin and end with the double spin-flip \hat{V}_1 .
- 3) Since the single-flip term \hat{V}_3 is the only one odd in the number of spin flips, any relevant term of the expansion must contain an even number of them.
- 4) We are looking for the lowest-order energy correction which lifts the degeneracy between classical ground states. The correction of the p th order associated with a specific linked cluster is given by

$$\delta E^{(p)} = \sum_{n_k} \frac{\langle 0|\hat{V}|n_1\rangle \langle n_1|\hat{V}|n_2\rangle \dots \langle n_{p-1}|\hat{V}|0\rangle}{(E_0 - E_{n_1}) \dots (E_0 - E_{n_{p-1}})}. \quad (53)$$

Here, E_0 is the classical ground-state energy and E_{n_k} are the unperturbed energies of excited states. This expression is straightforwardly obtained from the Brillouin-Wigner theory by replacing the exact ground-state energy E with E_0 , which is justified because E_{n_k} are the same for all classical ground states.

Degeneracy lifting

The degeneracy of the ordering patterns in the kagomé-lattice antiferromagnet is illustrated in Figs. 7(a) and (b). For a fixed spin triad in the lower triangle, spin \mathbf{S}_2 can be parallel either to spin \mathbf{S}_3 or $\mathbf{S}_{3'}$ of the upper triangle, having ferromagnetic-like or antiferromagnetic-like alignment of the second-neighbor spins. Extended over the entire lattice, the two structures correspond to the $\sqrt{3} \times \sqrt{3}$ and $\mathbf{q} = 0$ states.

According to the rules formulated above, the lowest-order correction distinguishing between the two patterns may appear only in the fourth order. An example of such a tunneling process is given by the operator sequence

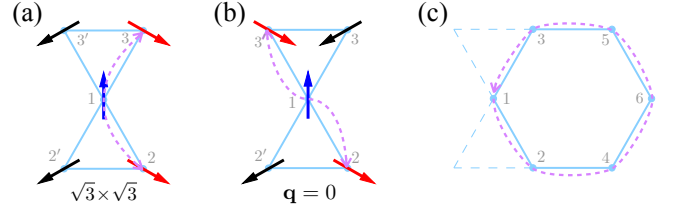


FIG. 7: Two degenerate spin configurations of the kagomé-lattice antiferromagnet with (a) ferromagnetic-like ($\sqrt{3} \times \sqrt{3}$) and (b) antiferromagnetic-like ($\mathbf{q} = 0$) arrangement of second-neighbor spins. (c) Smallest cluster with nontrivial topology contributing to the energy difference between states (a) and (b) in the 7th order of expansion. Schematics of the tunneling processes are also shown.

acting on the ground state from left to right

$$\hat{V}_1^{12} \rightarrow \hat{V}_3^{13} \rightarrow \hat{V}_3^{12} \rightarrow \hat{V}_1^{13}, \quad (54)$$

see Fig. 7(a). The respective energy shift depends explicitly on the mutual orientation of \mathbf{S}_2 and \mathbf{S}_3 because $\delta E^{(4)} \propto \sin \theta_{12} \sin \theta_{13}$. However, an obvious symmetry leaves the degeneracy intact at this order of expansion, because for any coupling between \mathbf{S}_2 and \mathbf{S}_3 there is a “mirror” counterpart to the tunneling process that couples \mathbf{S}_2 with $\mathbf{S}_{3'}$ identically, see Fig. 7(b), yielding $\delta E^{(4)} \propto \sin \theta_{12} \sin \theta_{13'}$. Since for any classical ground state $\sin \theta_{13'} = -\sin \theta_{13}$, the two processes provide the same energy gain to both $\sqrt{3} \times \sqrt{3}$ and $\mathbf{q} = 0$ states.

Generalizing this trend to the higher-order terms having the form $\delta E^{(p)} \sim \sin \theta_{12} \sin \theta_{13}$, we conclude that the processes represented by the graphs with trivial topology, i.e. connecting sites 2 and 3 via site 1 only, have to be discarded because there always exists a mirror graphs that connect site 2 and $3'$ via precisely the same process.

Therefore, the tunneling paths which lift the degeneracy between $\sqrt{3} \times \sqrt{3}$ and $\mathbf{q} = 0$ states must have a non-trivial topology, with the shortest one making a loop around a hexagon, see Fig. 7(c). Because such processes also need to be proportional to $\sin \theta_{12} \sin \theta_{13}$, they appear in the seventh order of expansion with one of the hexagon sides containing a double link. A simple analysis shows that the double link must be located on one of the two bonds: (1,2) or (1,3). According to the rules formulated above, all relevant seventh-order perturbation terms have to contain two double-flips \hat{V}_1 and two single-flips \hat{V}_3 , the latter acting only on bonds (1,2) and (1,3). Then, the remaining three links must contain either double spin-flip \hat{V}_1 or spin-flip hopping \hat{V}_2 —the fourth term in (52), \hat{V}_4 , does not contribute to this order in $1/S$.

Note that there are close parallels between the non-linear SWT and the real-space approach. Although the degeneracy-lifting contribution in the latter is of seventh order, it is still of second order in the cubic terms \hat{V}_3 , same as in the non-linear SWT (39).

The number of double-flips \hat{V}_1 or spin-flip hoppings \hat{V}_2

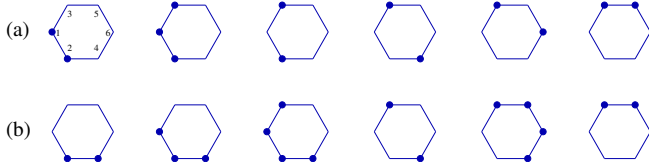


FIG. 8: Intermediate excited states of the 7th order tunneling process involving hexagon cluster generated by different operator sequences: (a) with three spin-flip hoppings, (b) without hoppings, all spin-flips. Position of spin flips is indicated by filled circles.

in a specific tunneling process determines the sign of the corresponding energy correction (53). In fact, according to (52), every double-flip operator carries a minus sign, whereas spin-flip hopping has a prefactor $(\Delta - \frac{1}{2})$, which is positive or negative depending on the value of Δ . For the seventh-order processes, denominator in (53) contains the product of six negative factors and is positive.

One example of the possible 7th order processes, which involves two double spin flips, two single flips, and three spin-flip hops, is given by the operator sequence (from left to right)

$$\hat{V}_1^{12} \rightarrow \hat{V}_3^{13} \rightarrow \hat{V}_3^{21} \rightarrow \hat{V}_2^{24} \rightarrow \hat{V}_2^{46} \rightarrow \hat{V}_2^{65} \rightarrow \hat{V}_1^{35}. \quad (55)$$

The intermediate stages of this perturbation process are shown in Fig. 8(a) where positions of spin flips is indicated by circles. Using $\hbar = 2JS$ and calculating the matrix elements we obtain

$$\delta E_a^{(7)} = -\frac{J}{2^{17} \cdot 3} (\Delta + \frac{1}{2})^2 (\Delta - \frac{1}{2})^3 \sin \theta_{12} \sin \theta_{13}. \quad (56)$$

One can also easily determine the respective multiplicative factor 2^5 associated with permutations of operators in (55), though our subsequent conclusions do not depend on precise numbers. For $\Delta > 1/2$, the energy correction (56) is negative and favors ferromagnetic alignment of second-neighbor spins, see Fig. 7(a), i.e., the $\sqrt{3} \times \sqrt{3}$ structure. For $\Delta < 1/2$, the energy correction changes sign and favors the $\mathbf{q}=0$ state of Fig. 7(b).

Clearly, $\Delta = 1/2$ is special, because the spin-flip hopping amplitude V_2^{ij} vanishes. At this value of anisotropy, the non-vanishing 7th order processes must involve only double spin flips and two single spin-flips. An example of such process is given by

$$\hat{V}_1^{24} \rightarrow \hat{V}_3^{21} \rightarrow \hat{V}_3^{13} \rightarrow \hat{V}_1^{12} \rightarrow \hat{V}_1^{56} \rightarrow \hat{V}_1^{46} \rightarrow \hat{V}_1^{35}, \quad (57)$$

with intermediate states shown in Fig. 8(b) and the energy shift

$$\delta E_b^{(7)} = \frac{J}{2^{19} \cdot 3} (\Delta + \frac{1}{2})^5 \sin \theta_{12} \sin \theta_{13}. \quad (58)$$

Straightforward but tedious calculation of the multiplicative factor attributed to (58) yields $176/3$. Because of

the positive sign, the correction $\delta E_b^{(7)}$ corresponds to the antiferromagnetic effective interaction between second-neighbor spins, Fig. 7(b), for the entire range $0 < \Delta < 1$. Hence, we can claim that for $\Delta = 1/2$ quantum fluctuations stabilize the $\mathbf{q}=0$ structure.

Furthermore, for $0 < \Delta < 1/2$, the spin-flip hopping amplitude V_2^{ij} has the same negative sign as V_1^{ij} , making the sign of all 7th-order perturbation processes contributing to the quantum energy shift the same, thus favoring the $\mathbf{q}=0$ state. We emphasize again that this conclusion relies only on the sign of the matrix elements and the order of the perturbation process, which, in turn, depends on the length of the shortest topologically nontrivial loop in the lattice. Thus, the quantum selection of the $\mathbf{q} = 0$ state for $0 < \Delta < 1/2$ stems from the lattice geometry.

For $\Delta > 1/2$, the perturbation terms with odd number of spin-flip hops change sign and favor the $\sqrt{3} \times \sqrt{3}$ state. This implies that the transition between the two magnetic structures can only happen at $\Delta_c > 1/2$ whose value must be determined by summing all contributions including corresponding multiplicative factors. This is, again, in accord with the answer from the second-order non-linear SWT, $\Delta_c \approx 0.72$.

Another close parallel between the non-linear SWT and the real-space approach is worth noting. The high order of the tunneling processes relevant to the degeneracy lifting explains the origin of the smallness of the quantum order-by-disorder effect. Since the real-space perturbation theory is, essentially, an expansion in coordination number ($z=4$ for the kagomé lattice), a rough but intuitively straightforward estimate of the seventh-order process, taking into account the number of next-nearest neighbor bonds and multiplicative factor of the symmetry-related processes, gives $\delta E = 8J/z^7 \approx 5 \cdot 10^{-4} J$ per spin. This is in a very good agreement with the results of SWT, $\approx 5 \cdot 10^{-4} J$ for $\Delta = 1/2$. Obviously, such a close quantitative agreement with the naive estimate is simply fortuitous. A more careful calculation for $\Delta = 1/2$, using our results in (58) with the combinatorial factor gives $\delta E \approx 1.1 \cdot 10^{-4} J$. This is in a good qualitative agreement with the SWT results and also implies that the higher-order “dressings” of the loop-like processes are quantitatively important.

A couple of additional remarks concern the “third-neighbor” effective interaction of spins 2 and 3', see Fig. 7. The corresponding linked cluster has one more link and hence appears only in the eighth order of perturbative expansion. Moreover, because of the even number of sites, all 8th-order processes must involve at least one spin-flip hopping operator \hat{V}_2 . Thus, for $\Delta = 1/2$ the 8th-order energy shift $\delta E^{(8)} \sim \sin \theta_{12} \sin \theta_{13'}$ vanishes and one has to go to the 9th order and the larger cluster. All that indicates that the $\mathbf{q} = 0$ spin structure should be stable with respect to the higher-order corrections.

-
- [1] A. B. Harris, C. Kallin, and A. J. Berlinsky, Phys. Rev. B **45**, 2899 (1992).
- [2] O. Cepas, C. M. Fong, P. W. Leung, and C. Lhuillier, Phys. Rev. B **78**, 140405 (2008).
- [3] L. Messio, O. Cepas, and C. Lhuillier, Phys. Rev. B **81**, 064428 (2010).
- [4] A. Chubukov, Phys. Rev. Lett. **69**, 832 (1992).
- [5] M. W. Long, J. Phys.: Condens. Matter **1**, 2857 (1989).
- [6] M. T. Heinilä and A. S. Oja, Phys. Rev. B **48**, 7227 (1993).
- [7] B. Canals and M. E. Zhitomirsky, J. Phys.: Condens. Matter **16**, S759 (2004).
- [8] D. L. Bergman, R. Shindou, G. A. Fiete, and L. Balents, Phys. Rev. B **75**, 094403 (2007); J. Phys.: Condens. Matter **19** 145204 (2007).
- [9] J. T. Chalker, P. C. W. Holdsworth, and E. F. Shender, Phys. Rev. Lett. **68**, 855 (1992).
- [10] R. J. Baxter, J. Math. Phys. **11**, 784 (1970).
- [11] D. A. Huse and A. D. Rutenberg, Phys. Rev. B **45**, 7536(R) (1992).